and similarly for mode n. In this case, the transforms are

$$\bar{X}_m(\beta) = \frac{2K(\cos\beta h_m - \cos Kh_m)}{\sin Kh_m(K^2-\beta^2)} \quad \text{(A15)}$$

$$\bar{Y}_m(f) = \frac{\sin(fw_m/2)}{(fw_m/2)}. \quad \text{(A16)}$$

Note that when (A15) and (A16) are substituted into (A12), the only place that the stagger between the modes enters is the factor $\cos\beta x_0 \cos fy_0$.

It should be noted that in evaluating (A9) or (A12) for real ϵ_{rc} (i.e., lossless slab), the integrand is singular when k satisfies

$$g\sinh gt + \epsilon_{rc}\gamma\cosh gt = 0. \quad \text{(A17)}$$

If ϵ_{rc} is complex (i.e., a lossy slab), then the values of k which satisfy (A17) are complex, and the integrand will be large but not singular. In either case, numerical integration in the vicinity of the singularity or near singularity will be difficult and time consuming. One should perform this region of the integral analytically using residue theory or similar techniques.

The right-hand vector in the moment-method solution is given by (6). Omitting all details, for a surface-patch mode center at the origin (i.e., mode J_m in Fig. 6) and J_i located at (x_f, y_f) the result is

$$V_m = \frac{j}{\pi\omega\epsilon_1}\int_0^\infty Q\int_0^{\pi/2}\beta\bar{X}_m\bar{Y}_m\sin\beta x_f\cos fy_f\,d\phi\,dk \quad \text{(A18)}$$

where

$$Q = \frac{k\gamma\sinh gt}{g(g\sinh gt + \epsilon_{rc}\gamma\cosh gt)}. \quad \text{(A19)}$$

References

[1] *IEEE Trans. Antennas Propagat*, vol. AP-29, Jan. 1981.

[2] N. G. Alexopoulos and I. E. Rana, "Mutual impedance computation between printed dipoles," *IEEE Trans. Antennas Propagat.*, vol. AP-29, pp. 106–111, Jan. 1981.

[3] E. H. Newman and P. Tulyathan, "Analysis of microstrip antennas using moment methods," *IEEE Trans Antennas Propagat.*, vol. AP-29, pp. 47–53, Jan. 1981.

[4] V H. Rumsey, "Reaction concept in electromagnetic theory," *Phys. Rev.*, vol. 94, no. 6, pp. 1483–91, June 1954.

[5] R. F. Harrington, *Field Computations by Moment Methods*. New York: MacMillan, 1968.

[6] E. H. Newman and D. M. Pozar, "Electromagnetic modelling of composite wire and surface geometries," *IEEE Trans Antennas Propagat*, vol. AP-26, pp 784–88, Nov. 1978.

[7] ——, "Considerations for efficient wire/surface modeling," *IEEE Trans. Antennas Propagat.*, vol. AP-28, pp. 121–124, Jan 1980.

[8] P. Silvester, "TEM wave properties of microstrip transmission lines," *Proc. IRE*, vol. 115, pp. 43–48, Jan. 1968.

[9] R. P. Jedlicka, M. T. Poe, and K. R. Carver, "Measured mutual coupling between microstrip antennas," *IEEE Trans. Antennas Propagat.*, vol. AP-29, pp. 147–149, Jan. 1981.

Analysis of the Hybrid Modes for an Eccentrically Cladded Fiber

ANDREAS D. LYRAS, JOHN A. ROUMELIOTIS, JOHN D. KANELLOPOULOS, AND JOHN G. FIKIORIS

***Abstract*—This paper examines the hybrid-cladding modes of an eccentrically cladded three-layer dielectric fiber. The solutions are specialized to small eccentricities, and exact closed-form expressions for the normalized deviations of the cutoff wavenumbers from those of the concentric case are determined. Numerical results for various types of hybrid-cladding modes of the fiber are given. For certain values of the parameters, it is possible to enhance the operating bandwidth of the basic hybrid mode HE_{11} over the conventional concentric fiber because its cutoff frequency can be shown to remain zero.**

Manuscript received June 25, 1982; revised July 5, 1983.

The authors are with the Department of Electrical Engineering, National Technical University of Athens, Athens 147, Greece.

I. Introduction

This paper extends the results of a previous work [1] for the symmetrical modes in a cladded fiber to the more interesting and practical case of its hybrid modes. The eccentricity d (Fig. 1) might arise either as a manufacturing defect or as an intentional feature of the fiber with the purpose of improving the operating characteristics. The main difference in the analysis of the two cases lies in the complexity of the limiting forms for the cutoff condition of the various hybrid modes. The same final expression for the cutoff wavenumbers of the cladding modes $k_{nm}(d)$ is obtained

$$k_{nm}(d) = k_{nm}(0)\left[1 + g_{nm}(k_{nm}(0)d)^2\right] \quad (1)$$

where for the normalized deviations g_{nm}, closed-form but more complicated expressions are developed. For certain values of the parameters, it is possible in conjunction with the results of [1] to enhance the operating bandwidth of the basic hybrid mode HE_{11} over the conventional concentric fiber. Numerical results for various hybrid modes and for several profiles of cladded fibers are also included.

II. The Analysis

Referring to the waveguide of Fig. 1, which is a perturbation of the more commonly known concentric structure and with assumed harmonic time dependence $\exp(i\omega t)$, the longitudinal field components $E_{z_1}^J(P)$ and $H_{z_1}^J(P)$ can be expanded in terms of the appropriate Bessel and azimuthal functions as follows:

$$\begin{bmatrix} E_{z_1}^1(P) \\ H_{z_1}^1(P) \end{bmatrix} = \sum_{n=0}^{\infty}\left[\begin{matrix}\alpha_n \\ \alpha_n'\end{matrix}\cos(n\theta_1) + \begin{matrix}\beta_n \\ \beta_n'\end{matrix}\sin(n\theta_1)\right]\cdot J_n(k_1r_1)e^{-i\gamma z} \quad (2)$$

$$\begin{bmatrix} E_{z_2}^1(P) \\ H_{z_2}^1(p) \end{bmatrix} = \sum_{n=0}^{\infty}\left\{\left[\begin{matrix}A_n \\ A_n'\end{matrix}J_n(k_2r_1) + \begin{matrix}B_n \\ B_n'\end{matrix}\quad B_n'Y_n(k_2r_1)\right]\cos(n\theta_1)\right.$$
$$\left. + \left[\begin{matrix}C_n \\ C_n'\end{matrix}J_n(k_2r_1) + \begin{matrix}D_n \\ D_n'\end{matrix}Y_n(k_2r_1)\right]\sin(n\theta_1)\right\}e^{-i\gamma z} \quad (3)$$

$$\begin{bmatrix} E_{z_3}^2(P) \\ H_{z_3}^2(P) \end{bmatrix} = \sum_{n=0}^{\infty}\left[\begin{matrix}A_{3n} \\ A_{3n}'\end{matrix}\cos(n\theta_2) + \begin{matrix}B_{3n} \\ B_{3n}'\end{matrix}\sin(n\theta_2)\right]$$
$$\cdot H_n^{(1)}(k_3r_2)e^{-i\gamma z} \quad (4)$$

where $k_i = (\omega^2\mu_i\epsilon_i - \gamma^2)^{1/2}$, $i = 1,2,3$. The superscript 1 or 2 denotes the reference center of coordinates (see Fig. 1). The subscript 1, 2, or 3 denotes the region of space.

The boundary conditions at $r_1 = R_1$ and $r_2 = R_2$ require that the tangential components of $\bar{E}, \bar{H}$ be continuous [1]. This further necessitates the re-expansion of the field components $E_{z_2}^1, H_{z_2}^1$ in terms of cylindrical circular wavefunctions around the axis 0_2 using translational addition theorems [2].

The end result is (4) and (5) of [1]. We then turn our attention to the hydrid modes of the fiber by considering values of $p \geq 1$, whereas the symmetrical modes of [1] correspond to $p = 0$.

0018-9480/83/1100-0945$01.00 ©1983 IEEE

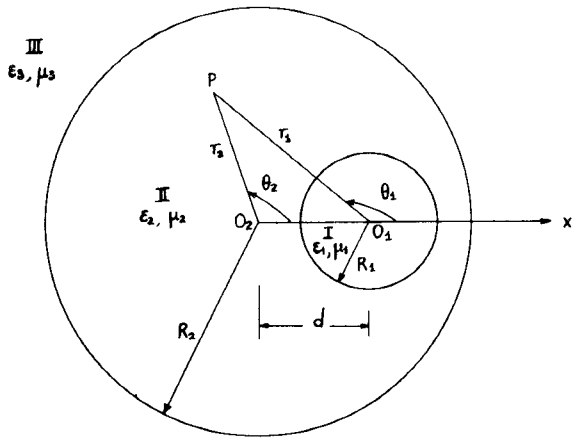

Fig 1. Cross section of the eccentric circular fiber

TABLE Ia
VALUES OF $u_{nm}(0)$ ($\epsilon_{r1} = 2.341$, $\epsilon_{r2} = 2.25$), $q = R_1/R_2$

mode	q = 0.05	q = 0.2	q = 0.4	q = 0.6	q = 0.8	q = 0.95
HE_{11}	0	0	0	0	0	0
HE_{21}	2.79568	2.79622	2.79152	2.77609	2.74975	2.72744
EH_{11}	3.83019	3.81027	3.77253	3.74717	3.72381	3.70514
HE_{12}	3.83170	3.83080	3.82021	3.79180	3.75017	3.71222
HE_{31}	4.28419	4.28412	4.28099	4.26021	4.21148	4.16958
EH_{21}	5.13562	5.13480	5.12495	5.09298	5.02855	4.97356
HE_{41}	5.61536	5.61534	5.61377	5.59289	5.51914	5.45948
HE_{22}	5.73123	5.72523	5.67630	5.61734	5.51987	5.51966
EH_{31}	6.38016	6.38003	6.37434	6.34016	6.25490	6.17956
HE_{51}	6.87539	6.87538	6.87469	6.85648	6.76919	6.68116
EH_{12}	7.01077	6.96325	6.91781	6.86031	6.82088	6.78468

TABLE Ib
VALUES OF g_{nm} (eHoE MODES)

mode	q = 0.05	q = 0.2	q = 0.4	q = 0.6	q = 0.8	q = 0.95
HE_{11}	-	-	-	-	-	-
HE_{21}	$-1.5\cdot10^{-2}$	$-1.6\cdot10^{-2}$	$-1.6\cdot10^{-2}$	$-1.5\cdot10^{-2}$	$-1.2\cdot10^{-2}$	$-9.5\cdot10^{-2}$
EH_{11}	$2.1\cdot10^{-4}$	$4.3\cdot10^{-3}$	$4.4\cdot10^{-3}$	$1.3\cdot10^{-3}$	$8.3\cdot10^{-4}$	$1.3\cdot10^{-3}$
HE_{12}	$1.8\cdot10^{-7}$	$-7.9\cdot10^{-5}$	$-3.4\cdot10^{-4}$	$-2.2\cdot10^{-3}$	$-3.3\cdot10^{-3}$	$5.2\cdot10^{-4}$
HE_{31}	$2.8\cdot10^{-3}$	$2.9\cdot10^{-3}$	$2.7\cdot10^{-3}$	$2.7\cdot10^{-3}$	$4.4\cdot10^{-3}$	$5.8\cdot10^{-3}$
EH_{21}	$-3.0\cdot10^{-5}$	$-2.1\cdot10^{-4}$	$4.4\cdot10^{-4}$	$2.1\cdot10^{-3}$	$-1.7\cdot10^{-4}$	$2.0\cdot10^{-3}$
HE_{41}	$6.3\cdot10^{-3}$	$7.5\cdot10^{-3}$	$7.3\cdot10^{-3}$	$6.8\cdot10^{-3}$	$8.4\cdot10^{-3}$	$9.9\cdot10^{-3}$
HE_{22}	$-9.5\cdot10^{-3}$	$-1.6\cdot10^{-2}$	$-1.2\cdot10^{-2}$	$-8.5\cdot10^{-3}$	$-2.6\cdot10^{-3}$	$-1.4\cdot10^{-2}$
EH_{31}	$-2.6\cdot10^{-6}$	$-1.6\cdot10^{-4}$	$-2.0\cdot10^{-4}$	$1.4\cdot10^{-3}$	$-2.4\cdot10^{-4}$	$1.7\cdot10^{-3}$
HE_{51}	$9.1\cdot10^{-4}$	$8.6\cdot10^{-3}$	$8.5\cdot10^{-3}$	$8.1\cdot10^{-3}$	$8.9\cdot10^{-3}$	$1.1\cdot10^{-2}$
EH_{12}	$3.9\cdot10^{-4}$	$1.3\cdot10^{-3}$	$4.5\cdot10^{-4}$	$3.1\cdot10^{-3}$	$2.3\cdot10^{-4}$	$6.9\cdot10^{-4}$
HE_{11}	-	-	-	-	-	-
HE_{21}	$-7.9\cdot10^{-3}$	$-8.6\cdot10^{-3}$	$-9.8\cdot10^{-3}$	$-8.9\cdot10^{-3}$	$-6.6\cdot10^{-3}$	$-4.4\cdot10^{-2}$
EH_{11}	$1.4\cdot10^{-4}$	$1.9\cdot10^{-3}$	$4.2\cdot10^{-3}$	$1.9\cdot10^{-3}$	$-7.5\cdot10^{-4}$	$4.2\cdot10^{-4}$
HE_{12}	$-9.5\cdot10^{-6}$	$-6.4\cdot10^{-5}$	$-5.2\cdot10^{-4}$	$-1.1\cdot10^{-4}$	$1.5\cdot10^{-3}$	$1.9\cdot10^{-3}$
HE_{31}	$1.3\cdot10^{-3}$	$1.6\cdot10^{-3}$	$8.9\cdot10^{-4}$	$-3.3\cdot10^{-4}$	$1.9\cdot10^{-3}$	$3.7\cdot10^{-3}$
EH_{21}	$-1.9\cdot10^{-7}$	$-1.0\cdot10^{-5}$	$2.4\cdot10^{-3}$	$-4.8\cdot10^{-3}$	$1.9\cdot10^{-3}$	$2.5\cdot10^{-3}$
HE_{41}	$4.3\cdot10^{-3}$	$4.5\cdot10^{-3}$	$4.2\cdot10^{-3}$	$3.2\cdot10^{-3}$	$4.3\cdot10^{-3}$	$6.3\cdot10^{-3}$
HE_{22}	$-8.6\cdot10^{-3}$	$-1.0\cdot10^{-2}$	$-6.7\cdot10^{-3}$	$-4.5\cdot10^{-3}$	$-1.7\cdot10^{-3}$	$-7.7\cdot10^{-2}$
EH_{31}	$-1.5\cdot10^{-8}$	$-3.0\cdot10^{-6}$	$1.8\cdot10^{-4}$	$-3.5\cdot10^{-3}$	$1.9\cdot10^{-3}$	$2.0\cdot10^{-3}$
HE_{51}	$3.3\cdot10^{-3}$	$5.3\cdot10^{-3}$	$5.3\cdot10^{-3}$	$4.4\cdot10^{-3}$	$4.9\cdot10^{-3}$	$7.2\cdot10^{-3}$
EH_{12}	$2.7\cdot10^{-4}$	$2.3\cdot10^{-3}$	$-2.5\cdot10^{-4}$	$1.4\cdot10^{-3}$	$5.0\cdot10^{-5}$	$-2.7\cdot10^{-4}$

In a cladded fiber, two main types of modes (cladding and core) propagate, each with the appropriate cutoff condition [3]. In each case, this condition suggests a particular limiting procedure for the evaluation of the various terms in the characteristic determinant of the problem [1]. Also, it may be noted here that apart from the symmetrical case [1], the modes of a concentric cladded fiber are, in general, hybrid, i.e., HE and EH. When the waveguide becomes eccentric, each type of HE/EH mode splits into what are called eHoE, oHeE and eEoH, and oEeH modes, in accordance with the angular symmetry of the E- and H-fields. They also correspond to the ETM, OTM, ETE, and OTE modes of metallic waveguides. More specifically, the oEeH and eHoE modes originate from the system of equations in (4) of [1], while the eEoH and oHeE ones originate from the system of equations in (5).

It can be shown further that the cutoff wavenumbers $k_{nm}(d)$ of the cladding modes have one-to-one correspondence and have values very near the $k_{nm}(0)$ of the concentric case ($n \geq 0, m \geq 1$). The line of reasoning is the same as in [2], but the limiting procedures are more involved, and the expressions are more lengthy and difficult to handle. The final result is expression (1), in which the g_{nm}'s are closed-form expressions, given in the Appendix.

It has also been shown analytically that the cutoff wavenumbers of the basic $(eHoE)_{11}$,$(oHeE)_{11}$ modes continue to remain zero, at least up to order $(k_2 d)^2$, where k_2 is the wavenumber of the field in region II (cladding). This fact also holds true in the concentric case. A corresponding result has also been obtained in the case of eccentric Goubau lines [2].

III. Numerical Results and Discussion

In this section, computed values of $u_{nm}(0) = k_{nm}(0) R_2$ and the corresponding values of g_{nm} are given for various hybrid modes and for several values of the parameters $q = R_1/R_2$, ϵ_{r1} (dielectric constant of core), and ϵ_{r2} (dielectric constant of cladding). They correspond to concentric fibers analyzed in [3] and extend to many more values of the parameters.

This analytical method for small eccentricities has already been applied in a variety of problems. An idea of its accuracy can be gained by referring to the case of the eccentric metallic waveguides [4], where comparisons with existing numerical and experimental results were possible.

After having proved that the cutoff equation for the hybrid cladding modes of the concentric cladded fiber, obtained as a special case in our analysis, is fully equivalent to (4) in [3], we have used the classification scheme for the hybrid modes proposed there to obtain numerical results for the ten lowest order hybrid cladding modes. The varying parameter is $q = R_1/R_2$ in Table Ia & b, while ϵ_{r1} and ϵ_{r2} vary in Tables II and III.

Since the cutoff frequency of the basic hybrid mode HE_{11} is shown to remain at zero, it is possible in certain cases to enhance the monomode operating bandwidth of this mode by increasing the cutoff frequency of the next higher mode TM_{01}, as has been pointed out in [1]. To give some numerical examples, we consider the TM_{01} mode in the case $\epsilon_{r1} = 2.341$, $\epsilon_{r2} = 2.25$, $q = 0.4$, $R_1 = 0.1$ mm, and $d/R_2 = 0.19$. From Table I in [1] we find the values $u_{01}(0) = 2.3798$ and $g_{01} = 2.7 \times 10^{-3}$. In this case, the cutoff frequency of the TM_{01} mode is $f_{01}(0) = 406.5$ GHz and the bandwidth increase is 0.22 GHz. In the case $\epsilon_{r1} = 5$, $\epsilon_{r2} = 2$, $q = 0.4$, $R_1 = 0.1$ mm, and $d/R_2 = 0.19$; the corresponding values are $u_{01}(0) = 1.7377$, $g_{01} = 0.0707$, and $f_{01}(0) = 331.9$ GHz, and the bandwidth increase is 2.55 GHz. For $q = 0.75$ (the other values of the parameters being the same), $u_{01}(0) = 1.3429$, $g_{01} = 0.1057$, and $f_{01}(0) = 256.5$ GHz. The bandwidth increase is 3.3 GHz. In general, the bandwidth increase becomes larger as $(n_1 - n_2)$ increases. Therefore, the eccentric cladded fiber may be advantageous over the concentric for monomode operation, particularly when only bandwidth considerations are to be taken into account.

Of course, it may be expected that the bandwidth enhancement will increase with the eccentricity, noticing that we are restricted here only to small values of kd. We further notice that the practical bandwidth of the HE_{11} mode should not be considered to extend down to zero frequency, but to be confined somewhere

TABLE II
$q = R_1/R_2 = 0.2$

	ϵ_{r1} = 2.3	ϵ_{r2} = 2.29		ϵ_{r1} = 2.3	ϵ_{r2} = 2.2999	
mode	$u_{nm}(0)$	g_{nm} eHoE	g_{nm} oHeE	$u_{nm}(0)$	g_{nm} eHoE	g_{nm} oHeE
HE_{11}	0	-	-	0	-	-
HE_{21}	2.80588	$-1.5\cdot10^{-2}$	$-7.5\cdot10^{-3}$	2.80821	$-1.2\cdot10^{-2}$	$-7.2\cdot10^{-3}$
EH_{11}	3.82939	$2.9\cdot10^{-4}$	$2.0\cdot10^{-4}$	3.83168	$2.9\cdot10^{-6}$	$2.1\cdot10^{-6}$
HE_{12}	3.83161	$-8.1\cdot10^{-7}$	$-6.5\cdot10^{-6}$	3.83170	$-8.0\cdot10^{-9}$	$-6.6\cdot10^{-8}$
HE_{31}	4.29398	$3.1\cdot10^{-3}$	$1.2\cdot10^{-3}$	4.29638	$2.1\cdot10^{-3}$	$9.8\cdot10^{-4}$
EH_{21}	5.13553	$-3.3\cdot10^{-5}$	$-9.6\cdot10^{-8}$	5.13562	$-3.8\cdot10^{-7}$	$4.2\cdot10^{-8}$
HE_{41}	5.62514	$6.6\cdot10^{-3}$	$4.1\cdot10^{-3}$	5.62752	$3.2\cdot10^{-3}$	$3.9\cdot10^{-3}$
HE_{22}	5.72793	$-1.6\cdot10^{-2}$	$-8.5\cdot10^{-3}$	5.73898	$-1.0\cdot10^{-3}$	$-8.1\cdot10^{-3}$
EH_{31}	6.38015	$-8.1\cdot10^{-7}$	$-1.5\cdot10^{-7}$	6.38016	$2.8\cdot10^{-7}$	$2.3\cdot10^{-8}$
HE_{51}	6.88506	$7.7\cdot10^{-3}$	$5.1\cdot10^{-3}$	6.88742	$5.4\cdot10^{-3}$	$4.9\cdot10^{-3}$
EH_{12}	7.00993	$2.9\cdot10^{-4}$	$2.5\cdot10^{-4}$	7.01555	$2.9\cdot10^{-6}$	$2.4\cdot10^{-6}$

TABLE III
$q = R_1/R_2 = 0.2$

	ϵ_{r1} = 5		ϵ_{r2} = 2
mode	$u_{nm}(0)$	g_{nm} eHoE	g_{nm} oHeE
HE_{11}	0	-	-
HE_{21}	2.72516	$-4.1\cdot10^{-2}$	$-4.3\cdot10^{-2}$
EH_{11}	3.29505	$6.7\cdot10^{-2}$	$6.2\cdot10^{-2}$
HE_{12}	3.79625	$-3.6\cdot10^{-3}$	$-5.0\cdot10^{-3}$
HE_{31}	4.21630	$-7.3\cdot10^{-4}$	$-2.3\cdot10^{-3}$
EH_{21}	5.11152	$3.0\cdot10^{-3}$	$3.6\cdot10^{-3}$
HE_{22}	5.47327	0.3465	0.4599
EH_{12}	5.51884	$-3.2\cdot10^{-2}$	$-3.6\cdot10^{-2}$
HE_{41}	5.54837	$5.3\cdot10^{-3}$	$3.3\cdot10^{-3}$
EH_{31}	6.37725	$1.9\cdot10^{-2}$	$1.6\cdot10^{-3}$
HE_{51}	6.80887	$6.5\cdot10^{-2}$	$4.3\cdot10^{-2}$

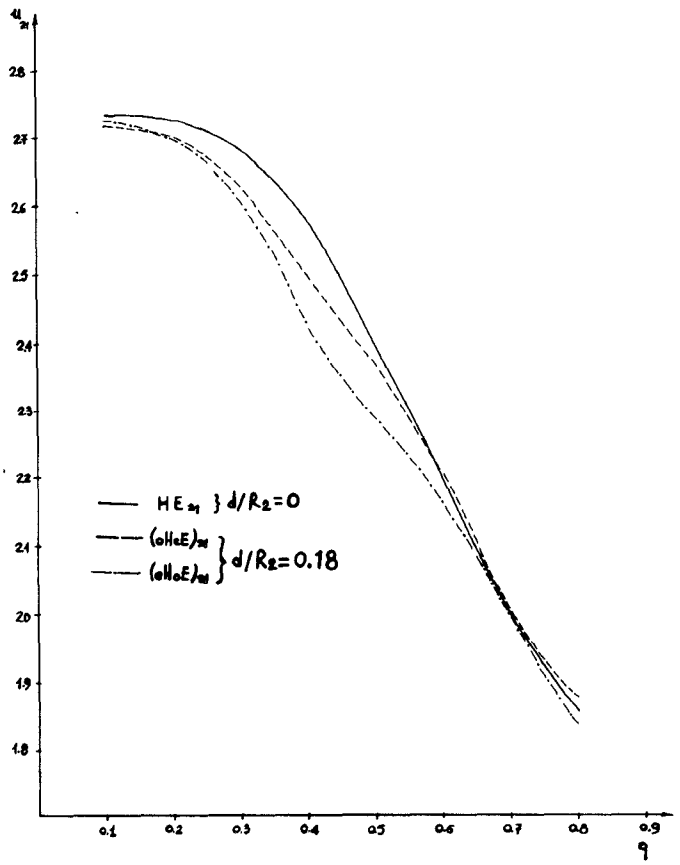

Fig. 2. Cutoff wavenumber variation versus $q = R_1/R_2$ for the HE_{21} mode of an eccentric cladded fiber ($\epsilon_{r1} = 5$, $\epsilon_{r2} = 2$, $d/R_2 = 0.18$).

around the operational range of the fiber. This implies that in evaluating the enhancement, the ratio of 3.3/256.5, in the last case, for instance, is meaningless.

Comparing the values of g_{nm} given in Tables Ib and III, we observe that these values are, in general, small when $n_1 \simeq n_2$ ($n_i = \epsilon_{ri}^{1/2}$) and become larger as $(n_1 - n_2)$ increases. Therefore, the eccentricity, considered as a manufacturing defect, is less important in large core/small Δ monomode fibers than in small core/large Δ ones.

We observe that when $n_1 \simeq n_2$ ($n_i = \epsilon_{ri}^{1/2}$), the g_{nm} of the oHeE modes are smaller than the corresponding coefficients of the eHoE modes. Quite the opposite is observed when n_1 and n_2 differ significantly. It should also be noticed that, in this case, the ordering of the modes on the basis of their cutoff frequency does change (Table III). Another useful observation is that the absolute values of g_{nm}, for all modes, become smaller as $q \to 0$ and $\epsilon_{r1} - \epsilon_{r2} \to 0$, while in the case $q \to 1$ they become larger. This is expected because as $q \to 1$, even a small eccentricity creates a large disturbance of the cross section of the fiber. We also observe that in all three cases, $q \to 0$, $\epsilon_{r1} - \epsilon_{r2} \to 0$, and $q \to 1$, the values of $u_{nm}(0)$ approach the well-known values for the dielectric rod.

In Fig. 2, the dependence of u_{nm} versus $q = R_1/R_2$ is shown for a cladded fiber with $\epsilon_{r1} = 5$ and $\epsilon_{r2} = 2$, for the concentric HE_{21} mode ($d/R_2 = 0$) and the eccentric $(oHeE)_{21}$ and $(eHoE)_{21}$ modes with $d/R_2 = 0.18$.

The chosen value of d/R_2 satisfies the physical limitation $d/R_2 \leq 1 - q$ for all values of q. In Fig. 3, the u_{nm} versus q is shown for a cladded fiber with $\epsilon_{r1} = 5$ and $\epsilon_{r2} = 2$, for the HE_{12} mode in the concentric case ($d/R_2 = 0$) and the $(oHeE)_{12}$ and $(eHoE)_{12}$ modes in the eccentric mode with $d/R_2 = 0.13$. Finally, in Fig. 4, the u_{nm} versus q is shown for a cladded fiber with $\epsilon_{r1} = 5$, ϵ_{r2}, for the EH_{11} mode in the concentric case ($d/R_2 = 0$), and the $(eEoH)_{11}$ and $(oEeH)_{11}$ modes in the eccentric one with $d/R_2 = 0.13$. These figures illustrate the observations made before. Comparing with Fig. 3 in [1], we further observe a remarkable similarity between the curves for the TE mode and the HE modes, as well as between the curves for the TM mode and the EH mode. This comparison confirms the prediction made in [1] that the hybrid Θ-dependent modes are more affected by the eccentricity. In Fig. 2, the fact is also illustrated that, for certain values of the parameters, the g_{nm} of a particular mode might be zero, e.g., for the $(oHeE)_{21}$ the g_{nm} becomes zero for $\epsilon_{r1} = 5$, $\epsilon_{r2} = 2$, and $q = 0.58$. In Fig. 3, we see that the g_{nm} of the $(oHeE)_{12}$ mode is zero for $\epsilon_{r1} = 2$, $\epsilon_{r2} = 2$, and $q = 0.425$, and the same is true for the g_{nm} of the $(eHoE)_{12}$ mode for $\epsilon_{r1} = 5$, $\epsilon_{r2} = 2$, and $q = 0.72$.

IV. Conclusion

The eccentrically cladded dielectric fiber is examined, in the case of small eccentricity. Exact closed-form expressions for the normalized deviations g_{nm} of the concentric fiber are given. Numerical results for the 10 lowest order hybrid modes are obtained. It turns out that, in certain cases, it is possible to enhance the monomode operating bandwidth of the basic mode HE_{11} over the concentric fiber.

Appendix

Throughout this Appendix, $J_n(t)$, $Y_n(t)$ and $n \geq 0$ are the Bessel functions, and $J_n'(t)$, $Y_n'(t)$, and $n \geq 0$ are their derivatives with respect to the argument.

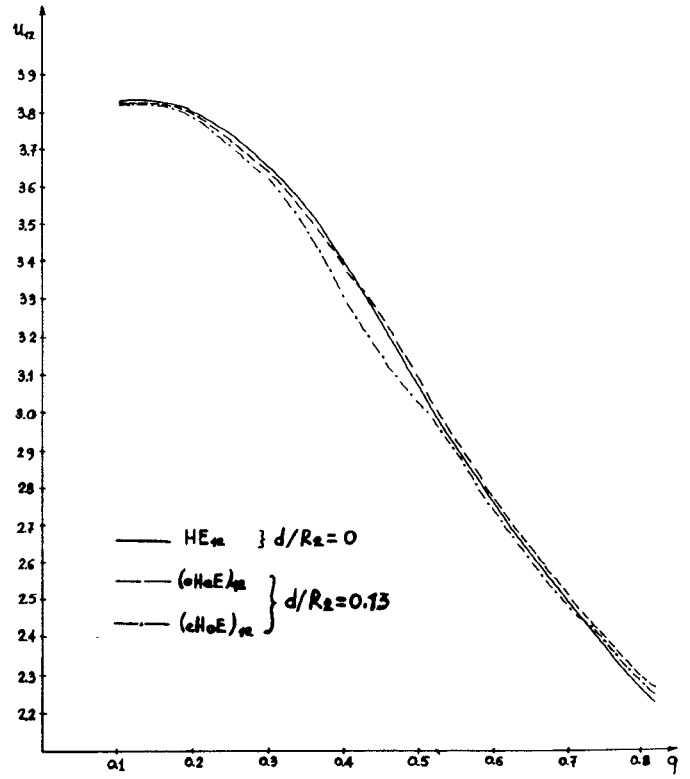

Fig. 3 Cutoff wavenumber variation versus $q = R_1/R_2$ for the HE_{12} mode of an eccentric cladded fiber ($\epsilon_{r1} = 5$, $\epsilon_{r2} = 2$, $d/R_2 = 0.13$).

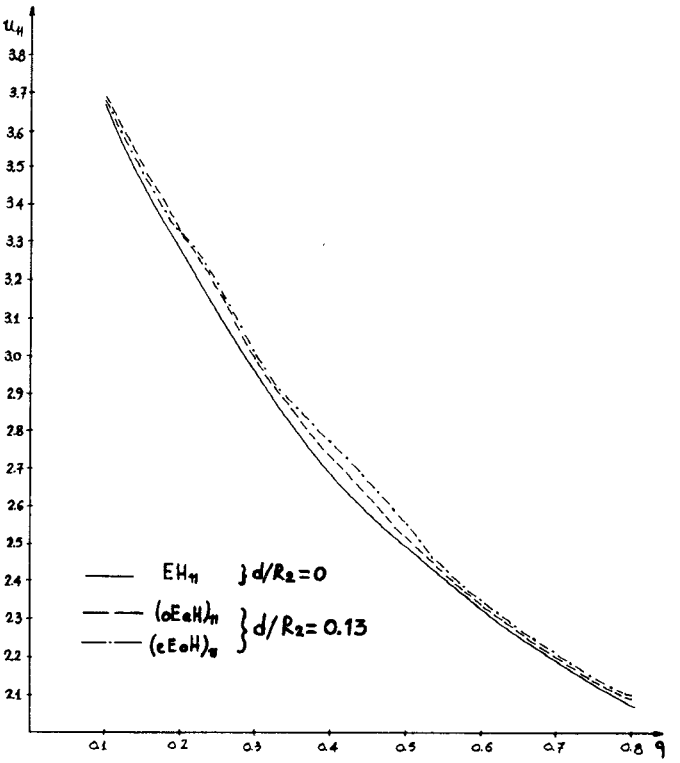

Fig. 4. Cutoff wavenumber variation versus $q = R_1/R_2$ for the EH_{11} mode of an eccentric cladded fiber ($\epsilon_{r1} = 5$, $\epsilon_{r2} = 2$, $d/R_2 = 0.13$).

The normalized deviations g_{nm} for the eHoE modes are given by the following closed-form expressions:

For $n = 1$

$$g_{1m} = \{u \cdot T_1(u)\}^{-1}\{G_{11}(u) + G_{21}(u) + G_{31}(u)\}, \qquad m \geq 1 \tag{A1}$$

where

$$u_{1m} = u_{1m}(0), \qquad m \geq 1 \tag{A2}$$

$$G_{11}(u) = \frac{K_{10} \cdot N_{B1} \cdot \left(J_0(u) \cdot Q'_{B11} - Y_0(u) Q'_{A11}\right)}{2 \cdot Q'_{B11} \cdot L_0} \tag{A3}$$

$$G_{21} = (u) = -\frac{SE_{21} \cdot \left\{Q'_{B22} \cdot (J_1(u) N_{B1} - Y_1(u) N_{A12}) + Q'_{A22}(N_{B12} - N_{B1}) Y_1(u)\right\}}{4 \cdot le_{22} \cdot Q'_{B11} \cdot Q'_{B22}} \tag{A4}$$

$$G_{31}(u) = \frac{Y_1(u)(N_{B12} - N_{B1})\left(Q'_{A21} Q'_{B11} - Q'_{B21} Q'_{A11}\right)}{4 \cdot Q'_{B11} \cdot Q'_{B22}} \tag{A5}$$

$$T_1(u) = dle_{11}/du. \tag{A6}$$

For $n > 1$

$$g_{nm} = \{u \cdot T_n(u)\}^{-1}\{G_{1n}(u) + G_{2n}(u) + G_{3n}(u) + G_{4n}(u)\}, \qquad m \geq 1 \tag{A7}$$

where

$$u = u_{nm}(0), \qquad m \geq 1 \tag{A8}$$

$$G_{1n} = -\frac{S_{En,n+1} \cdot S_{En+1,n}}{4 \cdot Q'_{Bnn} \cdot Q'_{Bn+1,n+1} \cdot le_{n+1,n+1}} \tag{A9}$$

$$G_{2n} = -\frac{S_{En,n+1} \cdot S_{En-1,n}}{4 \cdot le_{n-1,n-1} \cdot Q'_{Bnn} \cdot Q'_{Bn-1,n-1}}, \qquad n > 2 \tag{A10}$$

and

$$G_{22} = le_{22} \cdot G_{21}/le_{11} \tag{A11}$$

$$G_{3n} = -\frac{S_{Fn,n+1} \cdot \left(Q'_{An+1,n} \cdot Q'_{Bnn} - Q'_{An,n+1} \cdot Q'_{Bn+1,n+1}\right)}{4 \cdot Q'_{Bnn} \cdot Q'_{Bn+1,n+1}} \tag{A12}$$

$$G_{4n} = -\frac{S_{Fn,n-1}\left(Q'_{An-1,n} Q'_{Bnn} - Q'_{An,n+1} Q'_{Bn+1,n+1}\right)}{4 \cdot Q'_{Bnn} Q'_{Bn-1,n-1}} \tag{A13}$$

$$T_n(u) = dle_{nn}/du. \tag{A14}$$

The definitions for the various symbols appearing in expressions (A1)–(A14) are the following.

We define

$$x=\rho\cdot c_0 u,\quad u_1=\rho u,\quad \bar{u}=u/(\delta_{r2}-1)^{1/2}$$
$$\delta=\delta_{r2}+1/(\delta_{r2}-1)^{1/2}$$

where

$$\rho=R_1/R_2,\quad \delta_{ri}=\epsilon_{ri}\mu_{ri}\qquad (i=1,2,3)$$
$$c_0=(\delta_{r1}-1/\delta_{r2}-1)^{1/2}.$$

We also define

$$C_{1n}=-\frac{n\pi(\delta_{r2}-\delta_{r1})\zeta}{2\epsilon_{r2}(\delta_{r1}-1)}\qquad C_{2n}=-\frac{\pi\rho^2(\delta_{r1}-1)\zeta}{2n\epsilon_{r2}(\delta_{r2}-\delta_{r1})}$$
$$n\geq 1 \quad \text{(A15)}$$

where $\zeta=(\mu_0/\epsilon_0)^{1/2}$.

We then define, for $n\geq 1$

$$A_{1n}=C_{2n}u^2\left[\delta_{r1}R^2J_nY_n+\delta_{r2}c_0^2J_n'Y_n'-c_0R\left\{\epsilon_{r2}\mu_{r1}J_nY_n'+\epsilon_{r1}\mu_{r2}J_n'Y_n'\right\}\right]-C_{1n}J_nY_n \quad \text{(A16)}$$

$$A_{2n}=C_{1n}J_n^2+C_{2n}u^2\left[\delta_{r1}R^2J_n^2+\delta_{r2}c_0^2(J_n')^2-c_0R(\epsilon_{r1}\mu_{r2}+\epsilon_{r2}\mu_{r1})J_n'J_n\right] \quad \text{(A17)}$$

$$B_{1n}=-C_{1n}Y_n^2+C_{2n}u^2\left[\delta_{r1}R^2Y_n^2+\delta_{r2}c_0^2(Y_n')^2-c_0R(\epsilon_{r1}\mu_{r2}+\epsilon_{r2}\mu_{r1})Y_n'Y_n\right] \quad \text{(A18)}$$

$$B_{2n}=-C_{2n}u^2\left[\delta_{r1}R^2J_nY_n+c_0^2\delta_{r2}J_n'Y_n'-c_0R\left\{\epsilon_{r2}\mu_{r1}J_n'Y_n+\epsilon_{r1}\mu_{r2}J_nY_n'\right\}\right]+C_{1n}J_nY_n \quad \text{(A19)}$$

where $R=J_n'(x)/J_n(x)$ and the argument of the J_n, Y_n, J_n', and Y_n' functions is u_1 everywhere.

Define now, for $n\geq 1, p, q\geq 1$

$$N_{xn}=J_n(u)X_{1n}+Y_n(u)X_{2n}$$
$$N_{xn}'=J_n'(u)X_{1n}+Y_n'(u)X_{2n} \quad \text{(A20)}$$
$$N_{xpq}=J_p(u)X_{1q}+Y_p(u)X_{2q}$$
$$N_{xpq}'=J_p'(u)X_{1q}+Y_p'(u)X_{2q} \quad \text{(A21)}$$

where $X=A, B$.

We then define, for $n\geq 1, p, q\geq 1$

$$Q_{xnn}=\bar{u}\left[N_{xn}+\zeta Z_{xn}\right],\qquad Q_{xnn}'=\bar{u}\left[Z_{xn}+(N_{xn}/\zeta)\right] \quad \text{(A22)}$$

$$Q_{xpq}=\bar{u}\left[N_{xpq}+\zeta Z_{xp}\right],\qquad Q_{xpq}'=\bar{u}\left[Z_{xp}+(N_{xpq}/\zeta)\right] \quad \text{(A23)}$$

where $X=A, B$ and $Z_{An}=J_n(u)$, $Z_{Bn}=Y_n(u)$.

We further have

$$C_{xnn}=\zeta\bar{u}\left[\frac{Z_{xn}}{2(n-1)}-\mu_{r2}\frac{Z_{xn}'}{u}\right]+\left(\frac{n}{2}\right)\cdot\delta\cdot\left(\frac{N_{xn}}{u}\right),\qquad n>1 \quad \text{(A24)}$$

$$C_{xnn}=(\bar{u}/\zeta)\left[\frac{N_{xn}}{2(n-1)}-\epsilon_{r2}\frac{N_{xn}'}{u}\right]+\left(\frac{n}{2}\right)\cdot\delta\cdot\left(\frac{Z_{xn}}{u}\right),\qquad n>1 \quad \text{(A25)}$$

$$C_{xpq}=\zeta\cdot\bar{u}\left[\frac{Z_{xp}}{2(p-1)}-\mu_{r2}\frac{Z_{xp}'}{u}\right]+\left(\frac{p}{2}\right)\cdot\delta\cdot\left(\frac{N_{xpq}}{u}\right),\qquad p>1,\quad q\geq 1 \quad \text{(A26)}$$

$$C_{xpq}'=(\bar{u}/\zeta)\left[\frac{N_{xpq}}{2(n-1)}-\epsilon_{r2}\frac{N_{xpq}'}{u}\right]+\left(\frac{p}{2}\right)\cdot\delta\cdot\left(\frac{Z_{xp}}{u}\right),\qquad p>1,\quad q\geq 1 \quad \text{(A27)}$$

where $X=A, B$ and $Z_{An}'=J_n'(u)$, $Z_{Bn}'=Y_n'(u)$.

We also have

$$K_{10}=J_1(u)-R_0Y_1(u),\qquad L_0=J_0(u)-R_0Y_0(u) \quad \text{(A28)}$$

where $R_0=J_0'(x)J_0(u_1)-c_0J_0(x)J_0'(u_1)/J_0'(x)Y_0(u_1)-c_0J_0(x)Y_0'(u_1)$.

Finally we have

$$le_{11}=J_1(u)N_{B1}-Y_1(u)N_{A1}$$
$$le_{nn}=\left(\frac{n}{\epsilon_{r2}-1}\right)\left(\epsilon_{r2}+1-\frac{u^2}{n(n-1)}\right)\left[Jn(u)N_{An}-Jn(u)N_{Bn}\right]+\frac{4}{\pi}\frac{\zeta}{(\epsilon_{r2}-1)}+\left(\frac{u}{\epsilon_{r2}-1}\right)\cdot\left[\mu_{r2}\left\{Y_n'(u)N_{An}+J_n'(u)N_{Bn}\right\}+\epsilon_{r2}\left\{Y_n(u)N_{An}'-J_n(u)N_{Bn}'\right\}\right] \quad \text{(A30)}$$

$$S_{Epq}=Q_{Bpq}'\left(Q_{Apq}C_{Bpq}'+Q_{Bpq}'C_{Apq}-Q_{Apq}'C_{Bpq}-Q_{Bpq}C_{Apq}'\right)+Q_{Aqq}'\left(Q_{Bpp}C_{Bpq}'+Q_{Bpq}'C_{Bpp}-Q_{Bpq}C_{Bpp}'-Q_{Bpp}'C_{Bpq}\right),\qquad p\neq q \quad \text{(A31)}$$

$$S_{Fpq}=Q_{Bpq}'C_{Bpq}+Q_{Bpq}C_{Bpp}'-Q_{Bpq}'C_{Bpp}-Q_{Bpp}C_{Bpq}',\qquad p\neq q \quad \text{(A32)}$$

The normalized deviations g_{nm} for the oHeE modes are given by the same closed-forms expressions after the interchange $\epsilon_i\leftrightarrow\mu_i$ $(i=0,1,2)$ is performed everywhere.

References

[1] N. M. Metrou, J. D. Kanellopoulos, J. A. Roumeliotis, and J. G. Fikioris, "Analysis of the symmetrical modes for an eccentrically cladded fiber," *IEEE Trans. Microwave Theory Tech*, vol. MTT-30, pp. 217–220, Mar. 1982.

[2] J. A. Roumeliotis and J. G. Fikioris, "Cutoff wavenumbers and the field of surface wave modes of an eccentric circular Goubau waveguide," *J. Franklin Inst.*, vol. 309, no. 5, pp. 309–325, May 1980.

[3] A. Safaai-Jazi and G. L. Yip, "Cutoff conditions in three layer cylindrical dielectric waveguides," *IEEE Trans. Microwave Theory Tech.*, vol. MTT-26, pp. 898–903, Nov. 1978.

[4] J. A. Roumeliotis, A. B. M. Siddique Hossain, and J. G. Fikioris, "Cutoff wavenumbers of eccentric circular and concentric circular-elliptic metallic waveguides," *Radio Sci.*, vol. 15, no 5, pp. 923–937, Sept.–Oct. 1980.

An Accurate Determination of Dielectric Loss Effect in Monolithic Microwave Integrated Circuits Including Microstrip and Coupled Microstrip Lines

D. MIRSHEKAR-SYAHKAL

Abstract—**For the first time, by a rigorous analysis, the performance of MIC planar transmission lines with lossy substrates can be studied accurately. The general structural shape chosen for the analysis includes infinitely thin metallic strips embedded within the layers of homogeneous dielectric substrates. The rigor of the analysis was guaranteed by the assumption of the propagation of an electromagnetic hybrid wave (i.e., TE+TM) along the planar transmission lines. An efficient computation was, however, achieved by implementing the spectral domain approach as the basis for the analysis. To test the analysis, phase constants, characteristic impedances, and attenuations, due to dielectric losses, were computed for microstrip and coupled microstrip lines. The results obtained were compared with those given previously by the spectral domain analysis in which dielectric losses were not included directly [1]. The comparison showed an excellent agreement between the two theories for low-loss substrates. However, for lossy substrates the present method is more accurate.**

I. Introduction

A new generation of microwave integrated circuits, the so-called "Monolithic Microwave Integrated Circuits" (MMIC), is under development. In MMIC, the aim is to integrate as many passive and active microwave components as possible on one single chip, in order to achieve the highest degree of compactness. This, of course, would be of great advantage where a large number of repeated circuits is required. Examples of this can be found, for instance, in active arrays of antenna.

Substrates used for MMIC are of the semiconductor type [2]. This is because the substrate should provide a ground for the fabrication of the active elements, as well as the passive components. Propagation of the electromagnetic waves through a semiconductor medium is usually subject to a large attenuation [3]. The loss of propagating energy in a semiconductor substrate is mainly due to the finite resistivity of the medium. For example, silicon can have resistivity varying between 100–1200 $\Omega\cdot$cm [3]. Therefore, substrates used in MIC with similar resistivities could dissipate energy equal to or greater than the energy dissipated in metallic parts, i.e., strips.

So far, the capability of the theories developed for computing the dielectric loss of planar transmission lines have been limited either by the assumption of the quasi-TEM waves propagation [4], [5], or, in some cases, by the very crude plane-wave approximation [6]. The first accurate analysis of dielectric loss in which the effect of dispersion was considered was introduced by Mirshekar-Syahkal and Davies [1], [7]. In this general analysis, a perturbation technique was developed in order to deal with planar structures with multidielectric layers leading to

$$\alpha_d = \frac{\omega \sum_{i=1}^{I} \epsilon_i \tan\delta_i \iint_{S_i} |\vec{E}_0|^2 \, ds}{2\,\mathrm{Re} \iint_S \vec{E}_0 \times \vec{H}_0^* \cdot d\vec{s}} \tag{1}$$

where $\vec{E}_0$ and $\vec{H}_0$ are the unperturbed (zero-loss) fields. In (1), I denotes the number of dielectric layers, ϵ_i, $\tan\delta_i$ and S_i are the i^{th} dielectric layer permittivity, loss tangent, and cross-sectional area, and ω and S represent the angular frequency and the total transmission-line cross-sectional area, respectively. $\vec{E}_0$ and $\vec{H}_0$ are determined through the generalized spectral domain technique. A computer program providing $\vec{E}_0$ and $\vec{H}_0$, and subsequently α_d, is already available [8].

Though expression (1) can adequately describe the attentuation of a mode along a planar transmission line for substrates with small $\tan\delta$, the accuracy of (1) is not known. Especially in very lossy dielectric substrates, it is not only the accuracy of α_d that is important, but the effect of dielectric loss on wave length and on characteristic impedance can also be of considerable significance, particularly where the coupling of two lines becomes a point of interest.

To alleviate the shortcomings of earlier theories, the generalized method developed in [1], [7] is further extended to include *a priori* a complex dielectric constant. This new extension of the generalized spectral domain technique is then examined by solving two common structures, microstrip and coupled microstrip, taking different loss values for their substrates. Through this examination, the accuracy of the perturbation equation (1) can be examined.

II. Theory

A generic cross section of an arbitrary multistrip multidielectric MIC planar transmission line is shown in Fig. 1(a). The metallic enclosure is the inevitable packaging cover, and, therefore, its effect on the propagation of the wave has to be counted in the analysis. It is assumed that the dielectrics are homogeneous and the thickness of the strips satisfies the relation

$$\text{skin depth} \ll \text{strip thickness} \ll \text{dielectric thickness}.$$

A good metallization for the strips, and the use of a good conductor for the enclosure, allows the assumption of a perfect conductor for the metallic parts. However, the loss due to imperfect conductors can be calculated through a perturbation expression given in [1]. For brevity, conductor loss analysis is excluded from the following theory.

Considering the dielectric layers, the dielectric loss for each homogeneous dielectric region can be represented by the imaginary parts of a complex dielectric constant, given by

$$\epsilon_i = \epsilon_i' - j\epsilon_i'' = \epsilon_i'(1 - j\tan\delta_i)$$

where

$$\tan\delta_i = \epsilon_i''/\epsilon_i'.$$

In the case of any loss-free dielectric, of course, $\epsilon_i = \epsilon_i'$ and $\tan\delta_i = 0$.

Due to the mixed dielectric boundary of the problem, an accurate analysis without the assumption of an electromagnetic hybrid wave (i.e., TE+TM) is not possible. Based on this rigor-

Manuscript received April 21, 1983; revised June 20, 1983.

The author is with the London Centre for Marine Technology, University College London, London WC1E 7JE England.

0018-9480/83/1100-950$01.00 ©1983 IEEE